MR Elastography Detection of Early Viscoelastic Response of the Murine Hippocampus to Amyloid β Accumulation and Neuronal Cell Loss Due to Alzheimer's Disease

Tonia Munder, MD,[1] Anna Pfeffer, DVM,[1] Stefanie Schreyer, MS,[1] Jing Guo, PhD,[2] Juergen Braun, PhD,[3] Ingolf Sack, PhD,[2] Barbara Steiner, MD,[1†]* and Charlotte Klein, PhD[1†]

Purpose: To investigate in vivo viscoelastic parameters related to early histopathological changes in the hippocampus and the cortex in early, preclinical Alzheimer's disease (AD) stages.

Materials and Methods: Magnetic resonance elastography (MRE) was applied to female APP23 mice, an established transgenic mouse model of AD, at three different stages early in disease progression. To investigate the potential therapeutic effects of physical, cognitive, and social stimulation on brain viscoelasticity and histopathological characteristics, MRE was also applied after exposing young APP23 mice to environmentally enriched cage conditions (ENR), for 1, 12, or 24 weeks, which corresponds to adolescent, young-adult, and adult age at the time of analysis.

Results: Viscosity in the hippocampus of APP23 mice is lower than in controls (CTR) ($P = 0.005$) and does not increase with age, as in CTR mice (adolescent vs. young-adult: $P = 1.000$, vs. adult: $P = 0.493$, young-adult vs. adult: $P = 1.000$). Hippocampal cell numbers decrease with disease progression in APP23 mice ($P < 0.001$). Elasticity in the hippocampus is also reduced in APP23 mice ($P = 0.024$) but increases ($P = 0.027$) with disease progression. ENR in APP23 mice transiently increased hippocampal cell numbers ($P = 0.002$) but not viscosity ($P = 0.838$).

Conclusion: MRE detects alterations in viscoelasticity in the hippocampus related to early histopathological changes in the APP23 mouse model of AD.

Level of Evidence 1

Magnetic resonance elastography (MRE) is a noninvasive tool to measure viscoelastic properties of biological tissues in vivo.[1,2] In the brain, viscoelasticity is determined by the different cell types, their density, mobility as well as their interaction with the extracellular matrix.[3,4] These variables differ in distinct brain regions in the healthy brain and even more significantly under pathological conditions, which may be reflected in the biomechanical properties of the tissue and hence represented in viscoelastic parameters.[5,6] Therefore, specific changes in brain viscoelasticity can be considered as a potential biomarker for diagnosis and prognosis of neuropathological diseases.

Human MRE studies have shown that brain viscoelasticity is reduced with physiological aging[5] and under pathological conditions such as Alzheimer's disease (AD),[7] multiple sclerosis,[8] normal pressure hydrocephalus,[6]

frontotemporal dementia,[9] glioblastoma,[10] and progressive supranuclear palsy.[11] However, the underlying neural substrate causing such alterations of the viscoelastic parameters of brain tissue is not fully understood. The first steps towards a correlation between viscoelastic changes and the histopathology have been made using animal models of neuropathological diseases. Studies in a murine stroke model[12] and in a model of Parkinson's disease[13,14] have shown a strong correlation between neuronal density and brain viscoelasticity in disease-related brain regions. In particular, MRE was sensitive to detect local cellular changes due to adult neurogenesis in a relatively small brain region, the hippocampus.[13]

A progressive loss of neuronal cells in limbic and associated cortical areas is a hallmark of neurodegenerative diseases such as AD and is associated with cognitive decline and memory loss.[15] Growing patient numbers due to the aging society have caused rising socioeconomic costs.[16] AD is histopathologically characterized by extracellular neuritic amyloid β plaques, aggregations of a protein of 40 (Aβ40) or 42 amino acids (Aβ42) that first accumulates inside the cells and is then externalized into the extracellular matrix, as well as intracellular neurofibrillary tangles, which consist of self-assembled hyperphosphorylated tau proteins.[17,18] Clinical symptoms usually begin when the limbic regions are affected, mostly hippocampus and later cortex that project to medial temporal lobe structures.[18,19] This causes interrupted episodic memory function resulting in learning and memory deficits. Diminished recall accuracy, impaired problem-solving and cognition emerge when neocortical regions are affected.[17,20,21] By the time treatment starts, the disease has already progressed due to late diagnosis. Histopathologically, intra- and extracellular amyloid depositions and neuronal cell loss can already be found long before any symptoms occur.[18,22] In addition, adult hippocampal neurogenesis has been experimentally shown to be impaired in the early stages of AD.[23,24] Such histopathological changes cannot be detected early enough with conventional neuroimaging methods, leading to delayed diagnosis and hence ineffective treatment. At present, AD can only be diagnosed by a combination of multiple modalities, including MRI, [18F]-fluorodeoxyglucose positron emission tomography (PET), cerebrospinal fluid biomarkers, clinical memory tests, and Amyloid-PET.[25,26] After diagnosis, medication to increase levels of glutamatergic and cholinergic neurotransmitters,[27] regular physical exercise, as well as the involvement in daily life problem-solving are known to decelerate disease progression.[27,28] In animal studies, this physical and cognitive stimulation is induced by large environmentally enriched cages (ENR) with changing interior arrangements and larger animal groups. This enforces constant adaptation to new surroundings and consequently improves cognition and social interaction. Histologically, ENR is known to

enhance adult neurogenesis in the hippocampus and to be neuroprotective in AD.[29,30] Furthermore, the correlation of MRI brain scans in humans presenting AD pathology with high education and cognitive stimulation showed that more challenging surroundings led to increased hippocampal volume.[31]

So far, AD still cannot be cured but its progression can be slowed down, even more so when the disease is detected at an early stage. Therefore, a reliable preclinical diagnosis, when intracellular amyloid β depositions disturb cell homeostasis and the first changes in hippocampal neurogenesis can be found,[24] is essential for treating AD patients more effectively. MRE has the potential to become such a preclinical diagnostic tool: it is noninvasive, in contrast to taking cerebrospinal fluid for determining AD biomarkers, and it provides high sensitivity and resolution power to detect local structural changes on a cellular level.[32,33] Therefore, using MRE as a screening method for patients at risk of the early stages of cognitive impairments is an interesting prospect.

In the present study, we aimed to correlate early histopathological changes in the hippocampus and the cortex, brain areas primarily affected at early AD stages, with alterations in viscoelastic parameters. This contributes to the establishment of MRE as a clinical tool for early diagnosis and prognosis of neurodegenerative diseases. Therefore, MRE was applied on female APP23 mice, an established and well-studied transgenic mouse model of AD, at three different stages early in disease progression. To also investigate the potential therapeutic effects of physical and cognitive stimulation on brain viscoelasticity and histopathological characteristics, MRE was also applied after exposing young APP23 mice to two different cage conditions: standard (STD) or enriched (ENR), for 1, 12, or 24 weeks.

MATERIALS AND METHODS

Animals

The animal experiments were approved by the local Animal Ethics Committee and carried out in accordance with the European Communities Council Directive of 22 September 2010 (10/63/EU).

For the experiments, 45 female 6-week-old transgenic APP23 mice with a C57BL/6J background (further referred to as APP23) (Forschungseinrichtung für experimentelle Medizin FEM, Berlin, Germany), expressing human APP751 cDNA with the Swedish double mutation under the murine THY-1, 2 promoter[34] and 39 female 6-week-old C57BL/6J (Charles River, Sulzfeld, Germany) mice as controls (further referred to as CTR) were used. The genotype was confirmed by polymerase chain reaction (PCR) following ear punches (primers: APP ct forward: 5′ GAA TTC CGA CAT GAC TCA GG 3′, APP ct reverse: 5′ GTT CTG CTG CTG CAT CTT CGA CA 3′). Animals were kept in a temperature- and humidity-controlled colony room and maintained on a light/dark cycle of 12/12h with ad libitum access to food and water.
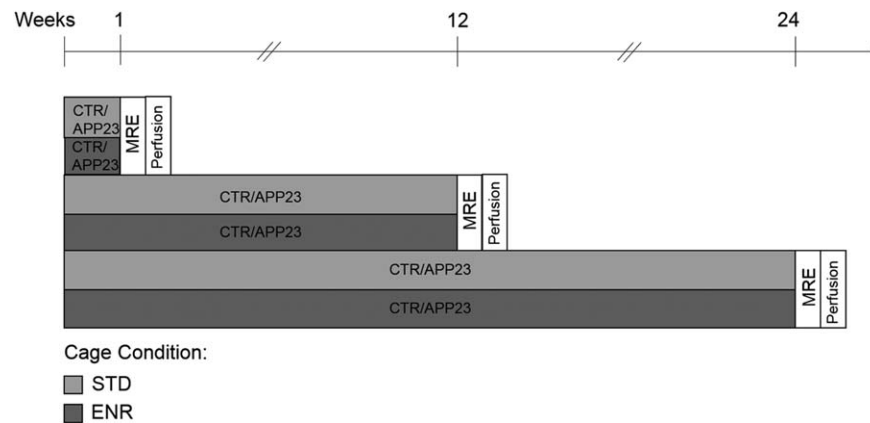
FIGURE 1: The experimental procedure for the MRE measurements, durations (1, 12, or 24 weeks = adolescent, young-adult, and adult as the final age) under standard (STD) or environmentally enriched (ENR) cage conditions and brain tissue perfusion for histological analyses.

Group Design and Experimental Procedure

Within each of the APP23 and CTR group, the mice were randomly cast into two different environmental modalities: STD cages ($n = 5$) under conventional laboratory conditions (Makrolon cages, $0.27 \times 0.15 \times 0.42$ m) and larger cages ($0.74 \times 0.3 \times 0.74$ m) for ENR ($n = 10$). Those ENR cages were equipped with tubes, cardboard boxes, and plastic houses, which were newly assembled weekly for physical and cognitive enrichment. In addition, more mice were housed in the ENR than in STD cages ($n = 10$ vs. 5) to also ensure social enrichment. The mice remained in their cages for either 1, 12, or 24 weeks (also referring to adolescent, young-adult, and adult age, respectively, at the time of analysis) until MRE measurement. To obtain baseline data of the viscous and elastic properties of hippocampal and cortical tissue, MRE was performed on 10 mice aged 6 weeks of both the APP23 and CTR group before they were placed into their assigned cages. In summary, mice of both genotypes (APP23 and CTR) were housed in two different cage conditions (STD and ENR) for three different durations (1, 12, or 24 weeks), resulting in 12 different experimental groups of $n = 5$–10 animals, which were submitted to MRE. The experimental procedure including the group design is shown in Fig. 1.

MRE

MRE was performed on a 7T MRI scanner (Bruker Pharma Scan, Ettlingen, Germany) running ParaVision Software 4.0 using a 20-mm diameter 1H-RF quadrature mouse volume coil as described before.[2] The mechanical vibration was generated by an air-cooled electromagnetic Lorentz coil triggered by the MRI scanner and transferred to the animal through a carbon fiber piston, which was connected to the bite bar transducer. The transducer was gimbaled through a rubber bearing and retaining bracket at the temperature-controlled mouse bed. A plastic disk held up the entire setup in the center of the magnet bore.

The timing of the vibration was defined and recorded by a fast low-angle shot (FLASH) sequence especially made for MRE measurement. The imaging sequence was altered for MRE by sinusoidal motion sensitizing gradient (MSG) in the through-plane direction with a strength of 285 mT/m, a frequency of 900 Hz, and 9 periods. To compensate for the static phase contributions, phase difference images were calculated from two images with opposite MSG polarity. Frequency amplitude and the number of sinusoidal oscillation cycles were controlled by a waveform generator connected via an audio amplifier to the driving coil. The main polarization of the vibration was transverse to the principal axis of the magnet field and the amplitudes were on the order of tens of micrometers. Further imaging parameters were: 128×128 matrix, 25×25 mm^2 field of view (FoV), 14.3 msec echo time (TE), 116.2 msec repetition time (TR), 8 time steps over a vibration period. Four axial slices with a thickness of 1 mm were acquired and the acquisition time was 20 minutes.

Complex wave images (Fig. 2B) corresponding to the harmonic drive frequency were extracted by temporal Fourier transformation of the unwrapped phase-difference images and filtered for suppressing noise and compression wave components. A 2D-Helmholtz inversion was performed, yielding the complex shear modulus G*. The regions of interest (ROIs), the hippocampus and cortex, were manually selected by outlining the anatomical structure from T_2-weighted (T_2w) MRI images (Fig. 2A). The tabulated spatially averaged G*-values are represented by the real part of the complex shear modulus G*, $G' = Re(G^*)$, known as the storage modulus that represents tissue elasticity (Fig. 2C), and the imaginary part $G'' = Im(G^*)$, which is the loss modulus and represents viscosity (Fig. 2D).[32]

Tissue Processing

Mice were killed the day after the MRE measurements. Animals were deeply anesthetized with ketamine/xylazine (10% ketamine hydrochloride, WDT; 2% Rompun, Provet, Lyssach, Switzerland; intraperitoneal injection) until they were unresponsive to toe and tail stock pinches. They were then transcardially perfused with 1M phosphate-buffered saline (PBS) and 4% paraformaldehyde (PFA). Brains were extracted and postfixed in PFA at 4°C overnight and then transferred into 30% sucrose for dehydration for 48 hours. Brains were frozen in 2-methylbutane cooled with liquid nitrogen and then cut into 40-μm thick coronal sections using a cryostat (Leica CM 1850 UV, Wetzlar, Germany). Brain sections were collected from bregma 2.2 mm to –4.0 mm and stored in 24-well plates containing cryoprotectant solution (25% glycerol, 25% ethylene glycol, and 50% 0.1M PBS) at 4°C until further use.
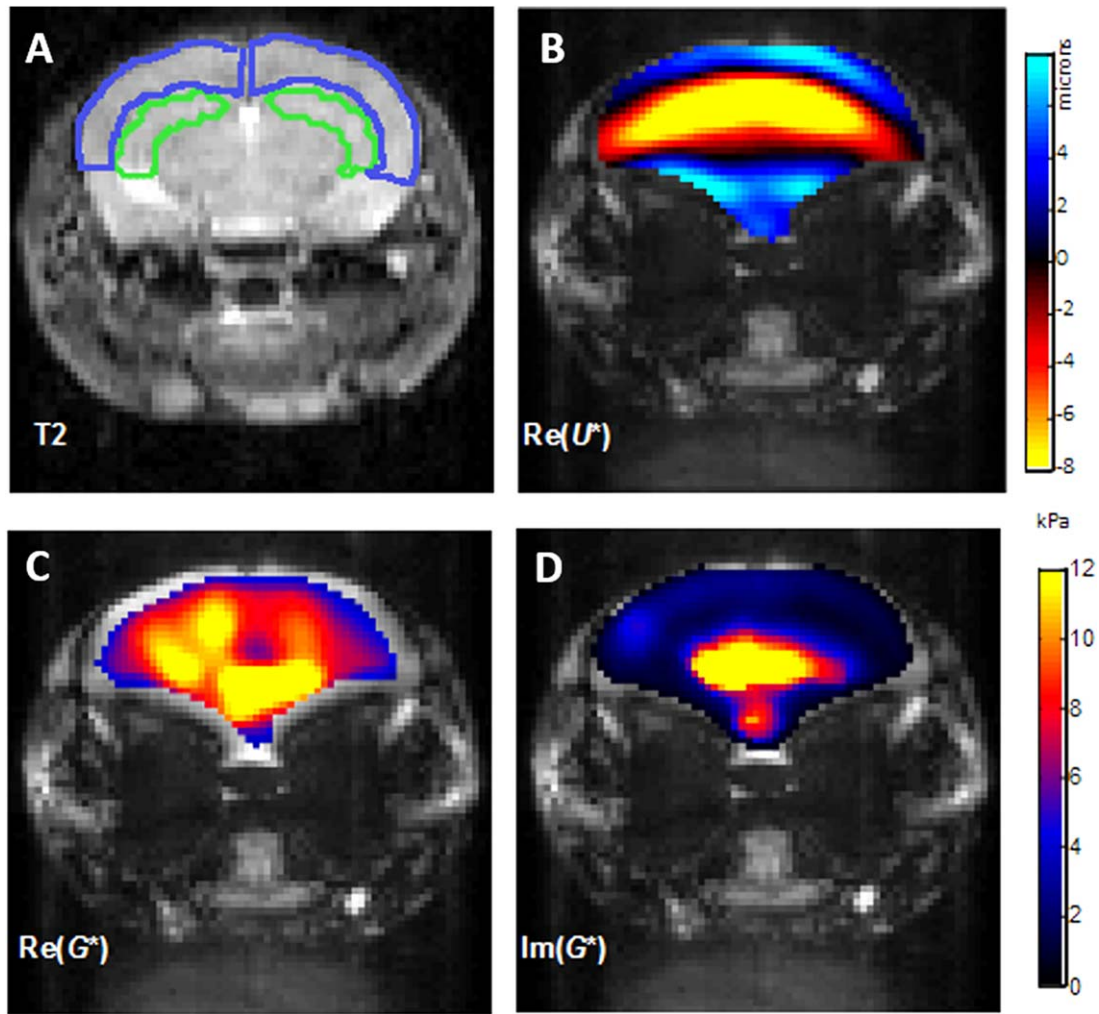
FIGURE 2: Representations of the T_2w MRI image (A), shear waves (B), storage (C), and loss modulus (D) maps in the mouse brain overlaid on the anatomic T_2w image. Regions of interest: cortex (blue line) and hippocampus (green line) were marked in T_2w-MRI.

Immunohistochemistry and Histology

AMYLOID β STAINING. Immunohistochemistry for the detection of intracellular amyloid deposits in the cortex and hippocampus was performed. Briefly, free-floating 1-in-12 section series were treated with 0.6% H_2O_2 to deactivate endogenous tissue peroxidases. After 30 minutes, background blocking with 3% donkey serum-enriched PBS (PBS+), sections were incubated with the primary antipurified Aβ_{17-24} antibody (1:1000, mouse; BioLegend, San Diego, CA) overnight at 4°C. The next day, after washing with PBS and blocking with PBS+, sections were incubated with biotinylated secondary antibody (1:250) for 2 hours at room temperature (RT). ABC reagent (Vectastain ABC Elite Kit, Vector Laboratories, Burlingame, CA) was applied for 1 hour. Ultimately, sections were incubated with diaminobenzidine (DAB) / peroxidase (Sigma, Germany) in a solution containing 0.3% H_2O_2 and 0.01% nickel chloride for at least 5 minutes at RT. Sections were mounted on microscope slides and coverslipped for later quantification.

DAPI STAINING. To determine the total cell number in the cortex and hippocampus, brain sections were stained with the fluorochrome 4′6-diamidino-2-phenylindole (DAPI), which binds to the DNA, thereby labeling cell nuclei. Free-floating 1-in-12-section series were rinsed and incubated with PBS-diluted DAPI (1:1000, Thermo Scientific, Waltham, MA) for 7 minutes, washed again, and afterwards mounted on microscope slides and coverslipped for later quantification.

CONGO RED STAINING. Tissue sections were washed with PBS and then mounted on slides. First, they were incubated for 5 minutes in matured hemalaun. Subsequently, they were put under running tap water for 10 minutes followed by exposure to solution 1a (saturated alcoholic sodium chloride solution: 2% NaCl in 80% ethanol, 1% aqueous NaOH per 100 mL) for 20 minutes. Then they were put in solution 2a (solution 1a with alkaline Congo red, Sigma-Aldrich) for 45 minutes. Here, the alkaline was added just before use. Afterwards they were washed, dehydrated, and mounted with a coverglass for later quantification.

Quantification of Plaque Load and Cell Numbers

STEREOLOGY. A Leica DMRE microscope equipped with StereoInvestigator (MicroBrightfield, Colchester, VT) software was used to quantify Aβ_{17-24}-positive (Aβ+) and DAPI-positive (DAPI+) stained cells. Aβ+ cells were counted separately in two brain areas, the cortex and the hippocampus, in both the right and

the left hemisphere of five APP23 mice of each cage and duration group. There was no Aβ immunoreactivity detected in the CTR group. The cells were traced with a 5× magnification objective in areas based on the mouse brain atlas between bregma –0.58 and –4.49 mm. Aβ+ cells were counted on every twelfth section with a 100× magnification objective in oil. The software randomly arranged counting frames of 60 × 60 × 60 μm with a sampling grid of 500 × 500 μm over the ROIs and an Optical Dissector height of 20 μm starting 5 μm below the top surface. The total number of cells per selected brain region was automatically calculated based on the settings described before from the manually counted cell numbers in the counting frames.

The same probe parameters were used for the quantification of DAPI+ cell nuclei in the hippocampus and cortex of mice of both genotypes, cage conditions, and all three durations, except that every sixth section was included. The DAPI+ cell nuclei in the hippocampus of five mice per group and three mice per group for the cortex were counted.

LIGHT MICROSCOPY. Extracellular plaques, visualized with Congo red, were counted manually with 200× magnification of a light microscope (Zeiss Axioskop, Germany) in the same areas as described above.

Statistical Analysis

Data were analyzed by applying a three-way analysis of variance (ANOVA) with factors genotype (g; CTR vs. APP23), cage (c; STD vs. ENR), and duration (d; 1 week vs. 12 weeks vs. 24 weeks or adolescent vs. young-adult vs. adult, respectively). To analyze the histological data of the Aβ staining in the APP23 mouse group, a two-way ANOVA with factors c and d was performed. In case of any interaction of the factors, pairwise comparisons were done using the Bonferroni post-hoc test. The relation between MRE parameters and histology in disease progression was analyzed using Pearson correlation. $P \leq 0.05$ was considered significant and trends of $P \leq 0.1$ are reported as descriptive. Graphical and statistical analyses were accomplished using GraphPad Prism 5.0 (San Diego, CA) and IBM SPSS statistics 19 (Armonk, NY).

RESULTS

Baseline-MRE of Hippocampus and Cortex Show Regional Differences in Elasticity: Hippocampus Has a Higher Elasticity Than Cortex

Mean values in the hippocampal region of the CTR group were 7.75 (±0.3) kPa and 1.16 (±0.13) kPa and of the APP23 mice 7.01 (±0.52) kPa and 1.21 (±0.11) kPa for G′ (elasticity) and G″ (viscosity), respectively. In the cortex, mean values of the CTR group were 2.60 (±0.33) kPa and 1.40 (±0.09) kPa and of the APP23 mice 2.62 (±0.34) kPa and 1.22 (±0.1) kPa for elasticity and viscosity, respectively. The hippocampus of both genotypes has generally higher values of elasticity than the cortex, which suggests a stiffer hippocampal tissue with no baseline differences between APP23 and CTR mice.

Hippocampus

VISCOSITY IN THE HIPPOCAMPUS OF APP23 IS REDUCED AND CELL NUMBERS DECREASE WITH AGE. The viscous properties of the hippocampus (Fig. 3B) in APP23 mice are

lower than in CTR mice (F(1,82) = 8.496, P = 0.005). A significant genotype × duration interaction (F(2,78) = 7.222, P = 0.001) indicates that the viscosity of hippocampal tissue in adult APP23 mice is reduced compared to CTR mice of the same age (P < 0.001). It also indicates that hippocampal viscosity of adult mice in the CTR group is higher than of adolescent (P = 0.001) and young-adult mice (P = 0.016). Such an age-dependent rise in viscosity cannot be observed in the hippocampus of APP23 mice.

A significant genotype × cage interaction (F(1,57) = 26.097, P < 0.001) indicates that the number of DAPI+ cells in the hippocampus (Fig. 3D) is lower in APP23 than in CTR mice in STD (P < 0.001). The duration further influences cell numbers (F(2,58) = 21.688, P < 0.001), indicating a decrease with age (1 vs. 12 vs. 24 weeks, P < 0.001). A significant genotype × duration interaction (F(2,55) = 4.575, P = 0.015) revealed that cell numbers are lower in adolescent and adult but not young-adult APP23 compared to age-matched CTR (CTR vs. APP23: P = 0.001 [adolescent] and P < 0.001 [adult]). A representative overview image of the DAPI-staining and a close-up image of hippocampal DAPI+ cells are shown in Fig. 5D,E, respectively.

The correlation of viscous values with DAPI+ cell numbers yielded a significant correlation only in APP23 mice under ENR cage conditions (r = 0.632, P = 0.011) (Supplemental Fig. S1A), indicating that higher cell numbers relate to an enhanced viscosity in hippocampal tissue.

HIPPOCAMPAL ELASTICITY IS REDUCED IN ADOLESCENT APP23 MICE BUT INCREASES WITH AGE. Elasticity in the hippocampus (Fig. 3A) increases with the duration (F(2,81) = 3.794, P = 0.027), indicating an age-dependent effect (1 week vs. 24 weeks: P = 0.031). A significant genotype × duration interaction (F(2,78) = 3.928, P = 0.024) revealed that hippocampal elasticity increases from adolescent to young-adult (P = 0.026) and to adult mice (P = 0.003) in the APP23 group, although the elastic values of adolescent APP23 mice were lower than in adolescent CTR mice (P = 0.018). Elasticity does not increase age-dependently in CTR mice (adolescent vs. young-adult: P = 0.648; adolescent vs. adult: P = 1.000; young-adult vs. adult: P = 0.260).

The quantification of Aβ+ cells in the hippocampus of APP23 mice (Fig. 3C) shows a trend towards an effect of duration on the amount of hippocampal cells containing accumulated amyloid β (F(2,28) = 3.199, P = 0.059), indicating a decrease from young-adult to adult mice (P = 0.057). Representative overview images of an Aβ-negative brain slice of a CTR mouse and of an Aβ+ brain slice of an APP23 mouse are shown in Fig. 5A,B. A representative close-up image of Aβ+ cells in the hippocampus representing intracellular amyloid β deposits is shown in Fig. 5C.

The correlation of elastic values with the number of Aβ+ cells yielded a significant correlation only in APP23
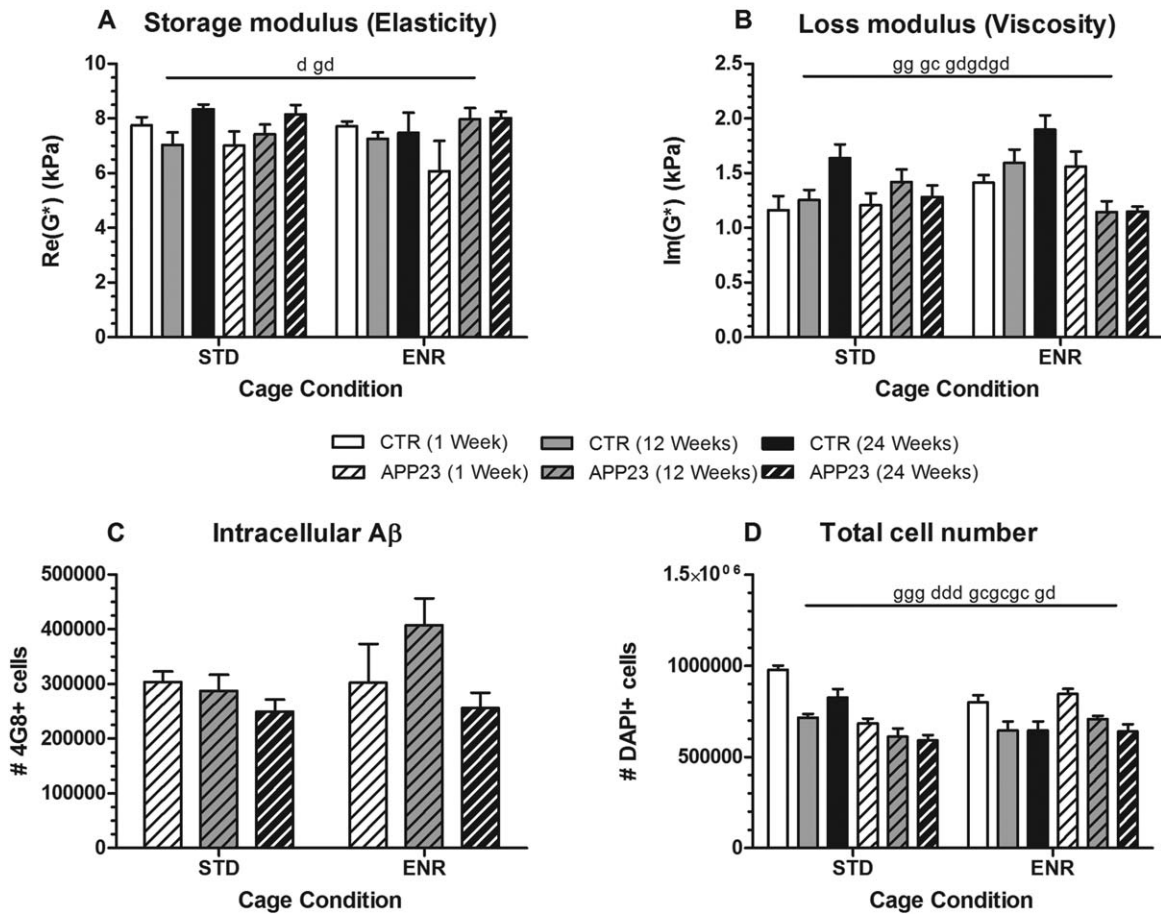
Hippocampus

FIGURE 3: Variations of MRE parameters (**A,B**) in the hippocampus of APP23 and CTR mice under standard (STD) or enriched environment (ENR) cage conditions of different durations (1, 12, or 24 weeks = adolescent, young-adult, or adult age) and respective numbers of Aβ+ cells (**C**; only in APP23 mice) and total cell numbers (**D**; DAPI+). Data are expressed as mean ± SEM. g = genotype, d = duration, gc = interaction of genotype and cage condition, gd = interaction of genotype and duration (d, gc, gd = *P* < 0.05; gg = *P* < 0.01; ggg, ddd, gcgcgc, gdgdgd = *P* < 0.001).

mice under ENR cage conditions (r = 0.536, P = 0.04) (Fig. S1B), indicating that increased amounts of cells accumulating Aβ are related to an enhanced elasticity in hippocampal tissue.

CELL NUMBERS BUT NOT HIPPOCAMPAL VISCOSITY IN APP23 MICE ARE INCREASED BY ENR. A significant genotype × cage interaction (F(1,80) = 4.798, P = 0.032) indicates that viscosity in the hippocampus (Fig. 3B) in the CTR group is increased after exposure to ENR (P = 0.007). This is not the case in APP23 mice (STD vs. ENR: P = 0.838).

In contrast, a significant genotype × cage interaction in the DAPI+ cell numbers (Fig. 3D) of the hippocampus (F(1,57) = 26.097, P < 0.001) reveals that in APP23 mice more cells can be found in ENR than in STD (P = 0.001). This leads to very similar cell levels in APP23 and CTR mice in ENR (P = 0.989). CTR mice in ENR, however, have fewer cells than in STD (P < 0.001). A trend towards a genotype × cage × duration interaction (F(2,54) =

2.822, P = 0.069) indicates that, compared to STD, ENR in APP23 mice increased the hippocampal cell numbers (1 week: P = 0.002) only transiently (12 weeks: P = 0.066; 24 weeks: P = 0.350).

No specific effect of ENR exposure on hippocampal elasticity is found in either CTR or APP23 mice (F(1,80) = 0.009, P = 0.926).

Cortex

CORTICAL VISCOSITY IS NOT AFFECTED IN APP23 MICE BUT CELL DENSITY DECREASES WITH AGE. Vis-. Viscosity in the cortex (Fig. 4B) is not different between CTR and APP23 mice (F(1,83) = 0.464, P = 0.498). However, the duration influences the number of cortical DAPI+ cells (Fig. 4D) (F(2,33) = 8.017, P = 0.002), indicating that it decreases with age (adolescent vs. young-adult and adult: P = 0.005 and P = 0.008, respectively). Fig. 5D shows a representative overview image of the DAPI staining in the cortex.

Cortex

A Storage modulus (Elasticity)

B Loss modulus (Viscosity)

Legend:
- □ CTR (1 Week) ■ CTR (12 Weeks) ■ CTR (24 Weeks)
- ▨ APP23 (1 Week) ▨ APP23 (12 Weeks) ▨ APP23 (24 Weeks)
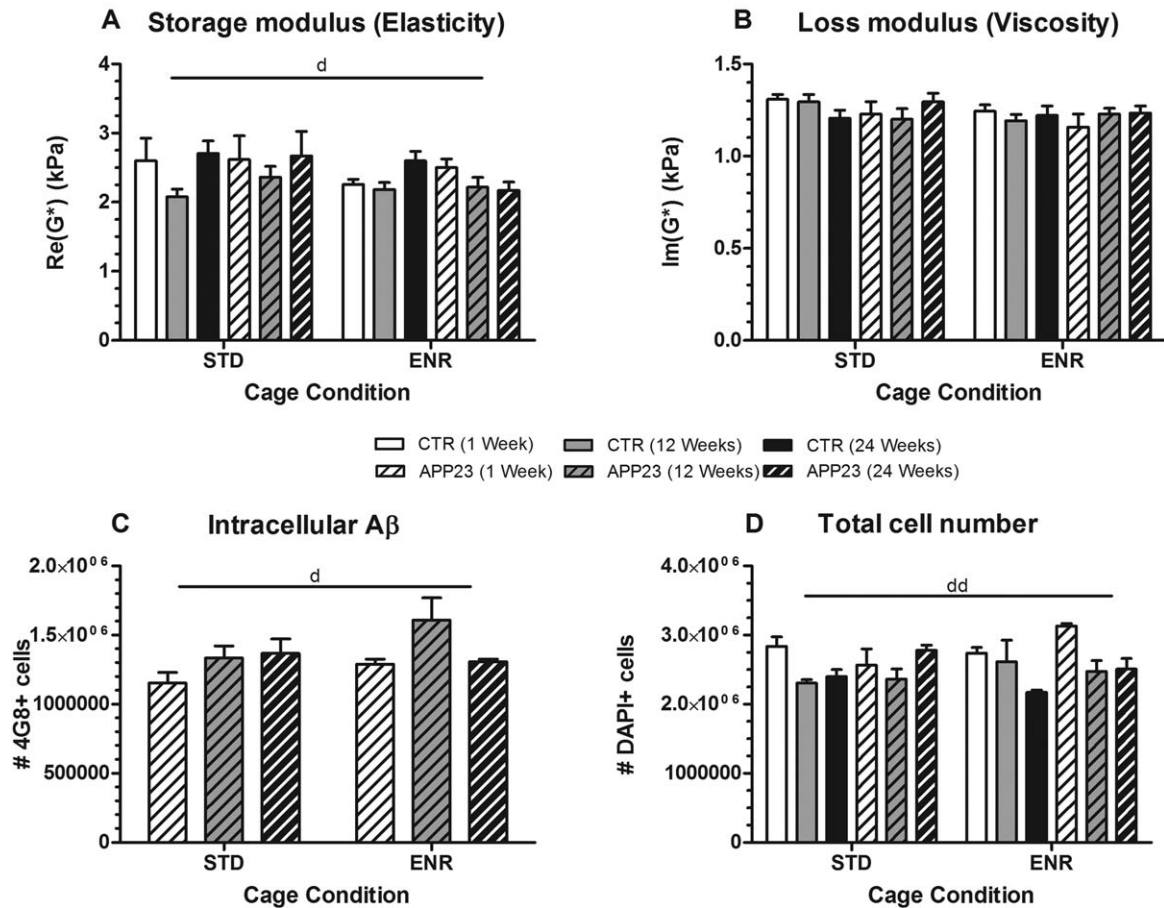
C Intracellular Aβ

D Total cell number

FIGURE 4: Variations of MRE parameters (A,B) in the cortex of APP23 and CTR mice under standard (STD) or enriched environment (ENR) cage conditions of different durations (1, 12, or 24 weeks = adolescent, young-adult, or adult age) and respective numbers of Aβ+ cells (C; only in APP23 mice) and total cell numbers (D; DAPI+). Data are expressed as mean ± SEM. d = duration (d = $P < 0.05$; dd = $P < 0.01$).

ENR had no effect on cortical viscosity in either CTR or APP23 mice ($F_{(1,81)} = 0.069$, $P = 0.794$).

No significant correlation was found between cortical viscosity and DAPI+ cell numbers in either genotype. A summary of the results is given in Supplementary Tables S1 and S2.

CORTICAL ELASTICITY INCREASES WITH AGE. In the cortex, a slight duration effect on the elastic properties (Fig. 4A) can be observed ($F_{(2,82)} = 3.242$ $P = 0.045$), indicating a trend towards an increase from young-adult to adult mice ($P = 0.063$).

An influence of duration is also seen in the amount of Aβ+ cells in the cortex of APP23 mice ($F_{(2,30)} = 3.660$, $P = 0.041$), indicating an increase from adolescent to young-adult mice ($P = 0.037$). Figure 5A,B shows representative overview images of an Aβ-negative brain slice of a CTR mouse and of an Aβ+ brain slice of an APP23 mouse, respectively.

No specific effect of ENR exposure on cortical elasticity can be observed in either CTR or APP23 mice ($F_{(1,81)} = 0.326$, $P = 0.570$).

No significant correlation was found between cortical elasticity and Aβ+ cells in either genotype. A summary of the results is given in Supplementary Tables S1 and S2.

DISCUSSION

In AD, histopathological changes such as intra- and extracellular amyloid β depositions and neuronal cell loss can be found long before any symptoms occur.[18,22] To date, detection of these changes at a preclinical stage of the disease is difficult, due to limitations of the presently available diagnostic modalities. An early diagnosis, however, is essential for treating AD patients more effectively. In the present study, we show that early histopathological changes in brain areas primarily affected in AD can be detected using MRE by capturing alterations in the biomechanical properties of the respective brain tissue.

We found that viscosity in the hippocampus of APP23 mice is lower than in CTR mice. In healthy animals, the viscous properties increase with age. This might be related to the increased number of mobile and unbound components due to brain modifications occurring within the time
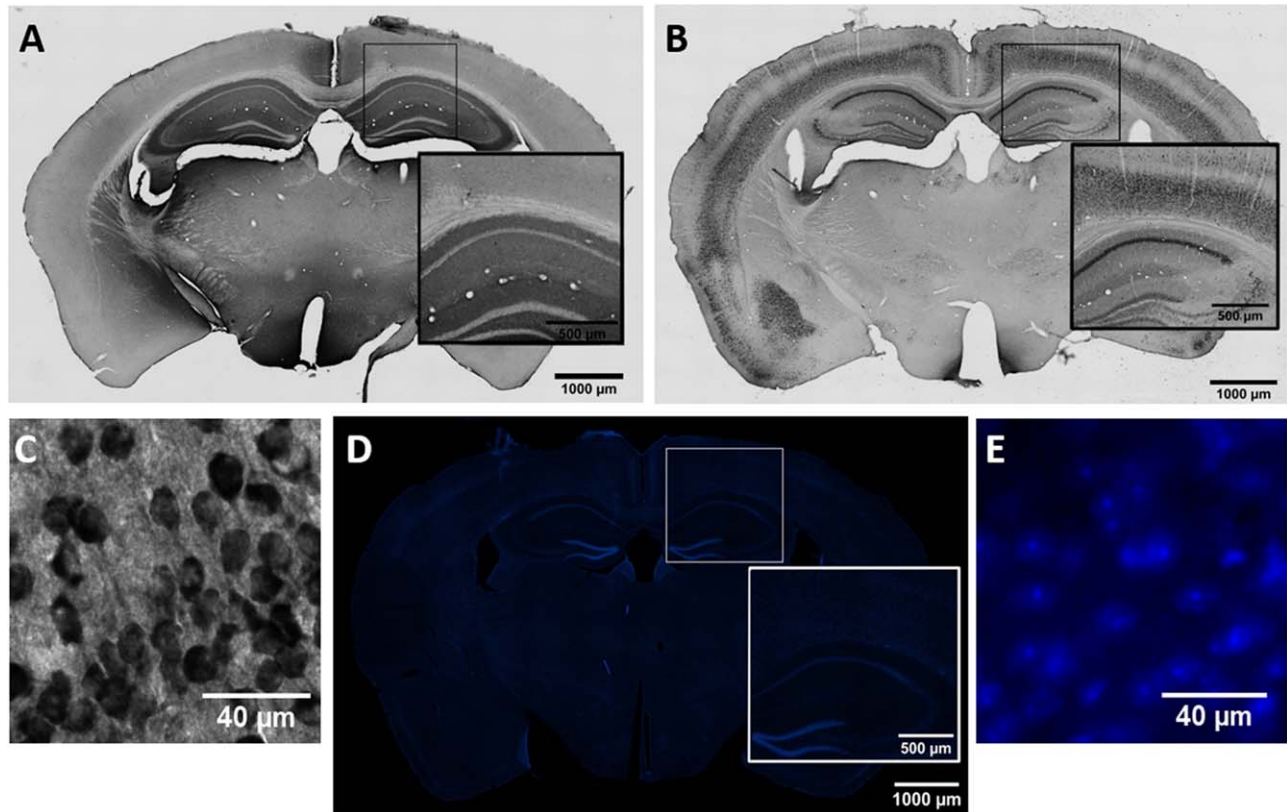
FIGURE 5: Representative microscope images of brain slices stained for intracellular amyloid β depositions using the $A\beta_{17\text{-}24}$ antibody (A–C) and for cell nuclei using DAPI (D,E), showing a $A\beta$-negative brain slice including the hippocampus and cortex of a CTR mouse (A), $A\beta+$ brain slice of an APP23 mouse (B), close-up view of $A\beta+$ hippocampal cells (C), DAPI-stained brain slice including the hippocampus and cortex of an APP23 mouse (D), and a close-up view of DAPI-stained hippocampal cell nuclei (E).

frame studied here. For instance, as the brain deteriorates due to aging, neuronal disintegration may result in a larger number of tissue elements, which are able to move in an incoherent way and thereby effectively absorb strain energy. Such a rise in viscosity does not occur in APP23 mice, indicating a disturbed or masked normal modification process in the brain, at least in the hippocampus, which is probably elicited by the progressive loss of neurons. In addition, elastic values in the hippocampus of adolescent APP23 mice are lower than in their healthy, age-matched counterparts. This also points towards very early pathological changes on the cellular level.

Furthermore, elastic and viscous properties in the hippocampus of APP23 mice are affected differently by AD during disease progression. The reduced hippocampal viscosity in APP23 mice, in particular adult animals compared to their healthy, age-matched counterparts, is probably due to the diminished neuronal functionality during AD.[35,36] In support of this hypothesis, Schwarb et al[37] linked the mechanical properties of human brain tissue with functional performance, which not only depends on structural but also functional integrity of the cellular network. However, such early dysfunction of the neurons and the network they build needs to be histologically studied in more detail in the APP23 mouse model. In contrast, the rise in elasticity

observed in APP23 mice in the present study may be linked to the slight but nonsignificant increased amount of hippocampal neurons showing intracellular accumulation of amyloid β and the subsequent appearance of extracellular amyloid β plaques due to the externalization of intracellular amyloid β. Supported by the significant positive correlation of elastic values to the amount of $A\beta+$ cells in APP23 mice under ENR, we hypothesize that the elastic properties of the hippocampus are increasing because more and more neurons accumulate amyloid β, before it is externalized into the extracellular matrix, where it could also affect the mechanical integrity of cells by filling the interstitial space in close contact with the cells. Moreover, intracellular accumulation of amyloid β has been shown to induce neuronal cell death.[38] We speculate that neurons that undergo apoptosis exhibit different biomechanical characteristics than healthy, fully functional neurons.

In the cortex, a similar but clearer increase in accumulating amyloid β within the neurons of APP23 mice over time can be found before it is externalized, leading to the appearance of extracellular amyloid β plaques. The appearance of amyloid β plaques in the old APP23 (at this point, 7–8 months old) is in accordance with other studies showing that extracellular plaque formation in the APP23 mouse model starts around 6 months of age.[34] However, other

than in the hippocampus, the slight but nonsignificant increase of cortical elasticity with age is independent of the genotype. Therefore, amyloid β accumulation in the cortex of APP23 mice cannot explicitly be associated with the elasticity in the cortex.

In a previous study, it has been shown that distinct brain areas in the mouse differ in their biomechanical properties.[14] The basic viscosity of the midbrain was higher than of the hippocampus, which we attributed to the higher proportion of white matter in the midbrain that has been shown to be stiffer than gray matter in the frequency range of MRE.[39,40] Here, we found that baseline elasticity of the hippocampus is higher than that of the cortex. Although the reason for these mechanical differences remains elusive, it may reflect their different anatomical structure. The hippocampus has several very densely packed cellular layers with axonal connections in between, whereas the cortex displays rather loosely packed cellular layers.

In the present study, we also investigated the potential therapeutic effects of physical, cognitive, and social stimulation on brain viscoelasticity and histopathological characteristics by exposing mice to ENR for different durations. We found that ENR was transiently effective in APP23 mice to increase the number of cells in the hippocampus, thereby keeping it on a higher level than in mice under STD cage conditions. However, similar to mice living in STD, a reduction over time due to disease progression can also be observed in ENR. The higher cell numbers might be due to the neuroprotective effects of ENR and/or due to enhanced neurogenesis in the dentate gyrus of the hippocampus.[29,30] Those mechanisms seem to transiently counteract the progressive cell loss until the process of cell loss becomes too severe to be effectively compensated any longer. Such a restorative effect is not seen in the viscous or elastic properties of the hippocampus, not even transiently. In CTR mice, however, ENR increases hippocampal viscosity, indicating that it has an influential effect on tissue mechanics. As the cell numbers in CTR, in contrast to APP23 mice, are not changed by ENR, the affected component of the tissue network accounting for the altered viscosity might be of a different character than just cellular. Moreover, this component can probably not be influenced by ENR any more or any influence is masked in APP23 mice due to the disease condition.

The present study is limited to APP23 mice as a model for AD and to female mice. Further thorough studies are required to estimate brain viscoelasticity in the early disease stages in other animal models of AD and in male subjects. In addition, a larger number of mice per group should be aimed at to affirm the tendencies seen here.

To summarize, we found that the elastic and viscous properties of hippocampal tissue are lower in APP23 mice at early disease stages compared to age-matched CTR mice. For viscosity, this difference becomes more pronounced with

disease progression. Furthermore, despite an initial increase in hippocampal cell numbers by ENR, exposure to ENR fails to stop the progression of neuronal loss and decrease in viscosity in the long term, indicating that it is therapeutically not suitable to prevent or halt the changes in tissue mechanical properties in AD.

In conclusion, our findings support previous work that MRE is sensitive to detect specific alterations in viscoelasticity, which occur on the cellular scale of brain tissue associated with early histopathological changes due to neurodegenerative processes. To our knowledge, this MRE study is the first to provide evidence of a disease-based difference in hippocampal viscosity preceding the AD-characteristic extracellular $A\beta$ pathology. Our study thereby contributes to the establishment of MRE as a clinical tool for early diagnosis and prognosis of neurodegenerative diseases.

ACKNOWLEDGMENT

REFERENCES

1. Muthupillai R, Ehman RL. Magnetic resonance elastography. Nat Med 1996;2:601–603.

2. Riek K, Klatt D, Nuzha H, et al. Wide-range dynamic magnetic resonance elastography. J Biomech 2011;44:1380–1386.

3. Lu Y-B, Franze K, Seifert G, et al. Viscoelastic properties of individual glial cells and neurons in the CNS. Proc Natl Acad Sci U S A 2006; 103:17759–17764.

4. Lu Y-B, Iandiev I, Hollborn M, et al. Reactive glial cells: increased stiffness correlates with increased intermediate filament expression. FASEB J 2011;25:624–631.

5. Sack I, Streitberger KJ, Krefting D, Paul F, Braun J. The influence of physiological aging and atrophy on brain viscoelastic properties in humans. PLoS One 2011;6.

6. Streitberger KJ, Wiener E, Hoffmann J, et al. In vivo viscoelastic properties of the brain in normal pressure hydrocephalus. NMR Biomed 2011;24:385–392.

7. Murphy MC, Huston J, Jack CR, et al. Decreased brain stiffness in Alzheimer's disease determined by magnetic resonance elastography. J Magn Reson Imaging 2011;34:494–498.

8. Wuerfel J, Paul F, Beierbach B, et al. MR-elastography reveals degradation of tissue integrity in multiple sclerosis. Neuroimage 2010;49: 2520–2525.

9. Huston J, Murphy MC, Boeve BF, et al. Magnetic resonance elastography of frontotemporal dementia. J Magn Reson Imaging 2016;43: 474–478.

10. Streitberger K-J, Reiss-Zimmermann M, Freimann FB, et al. High-resolution mechanical imaging of glioblastoma by multifrequency magnetic resonance elastography. PLoS One 2014;9:e110588.

11. Lipp A, Trbojevic R, Paul F, et al. Cerebral magnetic resonance elastography in supranuclear palsy and idiopathic Parkinson's disease. NeuroImage Clin 2013;3:381–387.

12. Freimann FB, Muller S, Streitberger KJ, et al. MR elastography in a murine stroke model reveals correlation of macroscopic viscoelastic

properties of the brain with neuronal density. NMR Biomed 2013;26: 1534–1539.

13. Klein C, Hain EG, Braun J, et al. Enhanced adult neurogenesis increases brain stiffness: In vivo magnetic resonance elastography in a mouse model of dopamine depletion. PLoS One 2014;9:1–10.

14. Hain EG, Klein C, Munder T, et al. Dopaminergic neurodegeneration in the mouse is associated with decrease of viscoelasticity of substantia nigra tissue. PLoS One 2016;11:1–16.

15. Nelson PT, Alafuzoff I, Bigio EH, et al. Correlation of Alzheimer disease neuropathologic changes with cognitive status: a review of the literature. J Neuropathol Exp Neurol 2012;71:362–381.

16. Alzheimer's Association. 2011 Alzheimer's disease facts and figures. Alzheimers Dement 2011;7:208–244.

17. Hardy J, Selkoe DJ. The amyloid hypothesis of Alzheimer's disease: progress and problems on the road to therapeutics. Science 2002; 297:353–356.

18. Selkoe DJ. Alzheimer's disease: genes, proteins, and therapy. Physiol Rev 2001;81:741–766.

19. Buckner RL, Snyder AZ, Shannon BJ, et al. Molecular, structural, and functional characterization of Alzheimer's disease: evidence for a relationship between default activity, amyloid, and memory. J Neurosci 2005;25:7709–7717.

20. Braak H, Braak E. Neuropathological stageing of Alzheimer-related changes. Acta Neuropathol 1991;82:239–259.

21. Braak H, Braak E, Bohl J. Staging of Alzheimer-related cortical destruction. Eur Neurol 1993;33:403–408.

22. Reiman EM, Caselli RJ, Yun LS, et al. Preclinical evidence of Alzheimer's disease in persons homozygous for the ε4 allele for apolipoprotein E. N Engl J Med 1996;334:752–758.

23. Demars M, Hu Y-S, Gadadhar A, Lazarov O. Impaired neurogenesis is an early event in the etiology of familial Alzheimer's disease in transgenic mice. J Neurosci Res 2010;88:2103–2117.

24. Haughey NJ, Nath A, Chan SL, Borchard AC, Rao MS, Mattson MP. Disruption of neurogenesis by amyloid beta-peptide, and perturbed neural progenitor cell homeostasis, in models of Alzheimer's disease. J Neurochem 2002;83:1509–1524.

25. Anand K, Sabbagh M. Amyloid imaging: poised for integration into medical practice. Neurotherapeutics 2017;14:54–61.

26. Health Quality Ontario. The appropriate use of neuroimaging in the diagnostic work-up of dementia: an evidence-based analysis. Ont Health Technol Assess Ser 2014;14:1–64.

27. Roberson ED, Mucke L. 100 years and counting: prospects for defeating Alzheimer's disease. Science 2006;314:781–784.

28. Schreiber S, Vogel J, Schwimmer HD, Marks SM, Schreiber F, Jagust W. Impact of lifestyle dimensions on brain pathology and cognition. Neurobiol Aging 2016;40:164–172.

29. Beauquis J, Pavía P, Pomilio C, et al. Environmental enrichment prevents astroglial pathological changes in the hippocampus of APP transgenic mice, model of Alzheimer's disease. Exp Neurol 2013;239: 28–37.

30. Hu Y-S, Xu P, Pigino G, Brady ST, Larson J, Lazarov O. Complex environment experience rescues impaired neurogenesis, enhances synaptic plasticity, and attenuates neuropathology in familial Alzheimer's disease-linked APPswe/PS1DeltaE9 mice. FASEB J 2010;24: 1667–1681.

31. Schröder J, Pantel J. Neuroimaging of hippocampal atrophy in early recognition of Alzheimer's disease — a critical appraisal after two decades of research. Psychiatry Res Neuroimaging 2016;247: 71–78.

32. Posnansky O, Guo J, Hirsch S, Papazoglou S, Braun J, Sack I. Fractal network dimension and viscoelastic powerlaw behavior: I. A modeling approach based on a coarse-graining procedure combined with shear oscillatory rheometry. Phys Med Biol 2012;57: 4023–4040.

33. Braun J, Guo J, Lützkendorf R, et al. High-resolution mechanical imaging of the human brain by three-dimensional multifrequency magnetic resonance elastography at 7T. Neuroimage 2014;90:308–314.

34. Sturchler-Pierrat C, Staufenbiel M. Pathogenic mechanisms of Alzheimer's disease analyzed in the APP23 transgenic mouse model. Ann N Y Acad Sci 2000;920:134–139.

35. Palop JJ, Chin J, Roberson ED, et al. Aberrant excitatory neuronal activity and compensatory remodeling of inhibitory hippocampal circuits in mouse models of Alzheimer's disease. Neuron 2007;55: 697–711.

36. Jang SS, Chung HJ. Emerging link between Alzheimer's disease and homeostatic synaptic plasticity. Neural Plast 2016;2016:7969272 [Epub ahead of print].

37. Schwarb H, Johnson CL, McGarry MDJ, Cohen NJ. Medial temporal lobe viscoelasticity and relational memory performance. Neuroimage 2016;132:534–541.

38. Kienlen-Campard P. Intracellular amyloid-beta 1-42, but not extracellular soluble amyloid-beta peptides, induces neuronal apoptosis. J Biol Chem 2002;277:15666–15670.

39. Kruse SA, Rose GH, Glaser KJ, et al. Magnetic resonance elastography of the brain. Neuroimage 2008;39:231–237.

40. McCracken PJ, Manduca A, Felmlee J, Ehman RL. Mechanical transient-based magnetic resonance elastography. Magn Reson Med 2005;53:628–639.